Yrast and near-yrast excitations up to high spin in $^{100}_{48}Cd_{52}$

R. M. Clark,[1] J. N. Wilson,[2,*] D. Appelbe,[3] M. P. Carpenter,[4] C. J. Chiara,[5] M. Cromaz,[1] M. A. Deleplanque,[1] M. Devlin,[2,†] R. M. Diamond,[1] P. Fallon,[1] D. B. Fossan,[5] R. V. F. Janssens,[4] D. G. Jenkins,[6] N. Kelsall,[6] T. Koike,[5] D. R. LaFosse,[5] G. J. Lane,[1] I. Y. Lee,[1] A. O. Macchiavelli,[1] D. G. Sarantites,[2] D. Seweryniak,[4] K. Starosta,[5] F. S. Stephens,[1] C. E. Svensson,[3,‡] K. Vetter,[1] R. Wadsworth,[6] J. C. Waddington,[3] D. Ward,[1] I. Wiedenhöver,[4] and B. Alex Brown[7]

[1]*Lawrence Berkeley National Laboratory, Berkeley, California 94720*

[2]*Chemistry Department, Washington University, St. Louis, Missouri 63130*

[3]*Department of Physics and Astronomy, McMaster University, Hamilton, Ontario, Canada L8S 4M1*

[4]*Argonne National Laboratory, Argonne, Illinois 60439*

[5]*Department of Physics and Astronomy, SUNY at Stony Brook, Stony Brook, New York 11794*

[6]*Department of Physics, University of York, Heslington, York, YO1 5DD, United Kingdom*

[7]*National Superconducting Cyclotron Laboratory and Department of Physics and Astronomy, Michigan State University, East Lansing, Michigan 48824*

(Received 19 August 1999; published 6 March 2000)

The gamma decay of excited states in the nucleus ^{100}Cd, which is two proton holes and two neutrons away from doubly magic ($N=Z=50$) ^{100}Sn, has been studied with the Gammasphere array following the ^{46}Ti(^{58}Ni,$2p2n$) reaction at 215 MeV. Residues were identified by detection of evaporated charged particles in the Microball CsI array, by neutron detection in a set of liquid scintillator detectors, and by a tag on the delayed gamma-ray decay of the known 8^+ isomeric state. The level scheme has been extended up to $20\hbar$ in angular momentum and to nearly 10 MeV in excitation energy. The results are compared with shell-model calculations.

PACS number(s): 21.10.−k, 23.20.Lv, 27.60.+j

In recent years, there has been an increasing experimental effort devoted to the study of nuclei near ^{100}Sn. This is because ^{100}Sn is the heaviest self-conjugate ($N=Z$) doubly magic nucleus accessible to experimental investigation [1–3]. Gamma-ray spectroscopic studies are edging ever closer to this goal but the very low (microbarn) cross sections and high backgrounds from other products in typical reactions present a considerable challenge that must be overcome. Experimental *tours de force* have recently identified excited states in $^{98}_{48}Cd_{50}$ [4] and $^{102}_{50}Sn_{52}$ [5,6] and these results have significance for our understanding of the origin of the effective interactions used in the shell-model description of nuclei.

The nucleus of interest in the present work is ^{100}Cd, which lies two proton holes and two neutrons away from $N=Z=50$. The level structure of this nucleus was previously established up to the $I^\pi=8^+$ isomeric [$t_{1/2}=60(3)$ ns] state formed from the $\pi g_{9/2}^{-2}$ configuration [7]. Below this isomer the 6_1^+ and 4_1^+ states are of predominantly neutron character while the 6_2^+ and 4_2^+ states, located closer in energy to the 8^+ isomer, are more consistent with a $\pi g_{9/2}^{-2}$ character. The clear separation of proton-hole and neutron-particle states indicates a very weak particle-hole neutron-proton residual interaction.

In this paper we report the results of a spectroscopic study of excited states in ^{100}Cd. The level scheme has been extended up to $20\hbar$ in angular momentum and to nearly 10 MeV in excitation energy. Comparison is made with a shell-model calculation based on the prescription outlined in [8], where the model space involves protons in the $2p_{1/2}$ and $1g_{9/2}$ orbits and neutrons in the $2d_{5/2}$, $3s_{1/2}$, $2d_{3/2}$, $1g_{7/2}$, and $1h_{11/2}$ orbits. An earlier shell-model calculation [9] with a more restricted model space (omitting the neutron $1h_{11/2}$ orbit) and with a slightly different choice of effective energies and operators is also compared with the data. We find that above angular momentum $\simeq 12\hbar$ the agreement between theory and experiment becomes worse. More sophisticated shell-model calculations are required and we hope that this paper will motivate such efforts.

Excited states in ^{100}Cd were populated in the ^{46}Ti(^{58}Ni,$2p2n$) reaction with a beam energy of 215 MeV. The beam, accelerated by the ATLAS accelerator at the Argonne National Laboratory, was incident on a target foil of $\simeq 1.0$ mg/cm^2 ^{46}Ti (86% enrichment). A catcher foil of $\simeq 12$ mg/cm^2 Au was placed immediately behind the target foil with the aim of stopping all recoils of interest and thereby allowing a tag on delayed gamma transitions coming from isomeric states. Gamma rays were detected with the Gammasphere array [10] which for this experiment comprised 88 large-volume ($\sim$75% efficient) Compton-suppressed Ge detectors. Channel selection was achieved by detecting evaporated light-charged particles in the 4π CsI array, Microball [11], and neutrons in 20 NE213 liquid scintillator detectors situated at the most forward detector positions of Gammasphere. The event trigger required detection of either at least one neutron plus two gamma rays or at least four gamma rays (which includes all gamma rays coming

*Present address: Niels Bohr Institute, Blegdamsvej 17, Copenhagen, Denmark.

†Present address: Los Alamos National Laboratory, Los Alamos, NM 87545.

‡Present address: Lawrence Berkeley National Laboratory, Berkeley, CA 94720.

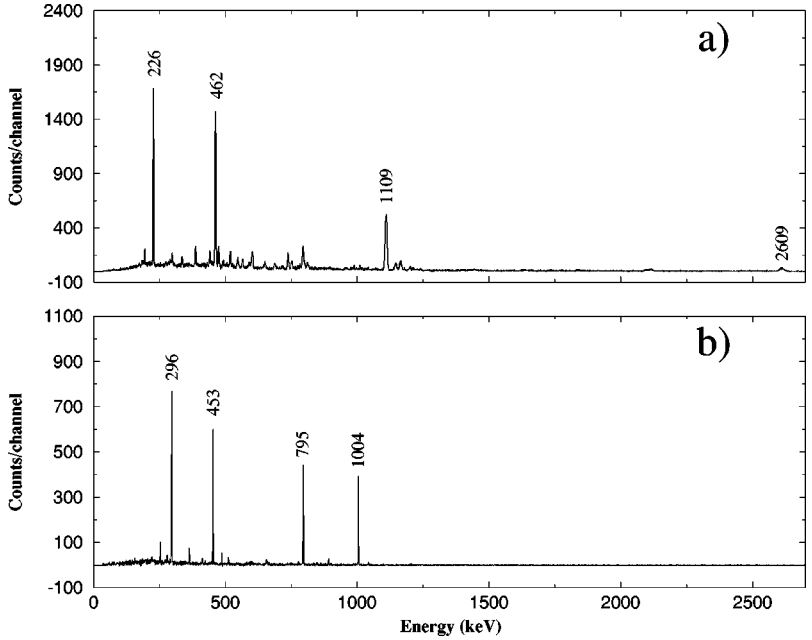

FIG. 1. (a) Prompt spectrum of gamma rays formed by a sum of coincidence gates placed on the 296, 453, 795, 1004 keV delayed gamma transitions beneath the isomeric 8^+ state in ^{100}Cd; (b) delayed spectrum of gamma rays formed from a single gate on the 1109 keV prompt transition seen in (a). Both spectra were created after channel selection, requiring the detection of two protons and at least one neutron (see text for details).

within $\simeq$800 ns of the initial beam burst, with successive beam pulses separated by $\simeq$80 ns). Protons and alpha particles were identified by Microball using two independent pulse-shape discrimination techniques [11]. Neutrons versus gamma rays were discriminated in the neutron detectors by pulse–shape analysis of signals as well as by time-of-flight determination.

A total of $\simeq 1.65\times 10^9$ events were collected and sorted off line into various channel-gated E_γ projections, E_γ-E_γ matrices, and E_γ-E_γ-E_γ cubes. For ^{100}Cd, which is formed via the $2p2n$ evaporation channel with an estimated cross section (by comparison with dominant residues) of $\simeq$5 mb, additional channel selectivity was achieved by requiring a coincidence with known gamma rays deexciting the 60 ns $I^\pi = 8^+$ state [7]. No transitions above this state were previously known. Shown in Fig. 1 are coincidence spectra created by gates on an E_γ(delayed)-E_γ(prompt) matrix formed by requiring the detection of two protons and at least one neutron. Here, E_γ(prompt) means that the gamma ray was detected within a $\pm$10 ns coincidence window set on the peak in a time spectrum formed from the distribution of the time differences between the detection of a Ge signal (the ''pretrigger'') and the associated beam pulse. E_γ(delayed) means that a gamma ray is detected within a $\pm$30 ns window centered between beam pulses. Figure 1(a) shows the prompt spectrum projected from a sum of gates on the 296, 453, 795, and 1004 keV delayed gamma rays beneath the 8^+ isomer in ^{100}Cd. The figure reveals several new transitions which presumably lie above the 8^+ isomeric level. Figure 1(b) presents the projected delayed spectrum formed from a single gate on the 1109 keV prompt gamma ray, and this clearly confirms its assignment to ^{100}Cd. In this way we were able to assign new transitions to ^{100}Cd. To build a level scheme, an E_γ(prompt)-E_γ(prompt) matrix was formed by incrementing events which were in coincidence with any of the four strong delayed transitions mentioned above. Note that this isomer gating was sufficiently clean that no other channel selection was required, thereby maximizing the statistics. Figure 2 shows a spectrum formed from a single gate on the 2609 keV line and illustrates the quality of the data. From this matrix we constructed the level scheme proposed in Fig. 3. All the transitions from states above the 8^+ isomer (marked by a thick line) were previously unknown. The energies and relative intensities of transitions below and above the isomer are summarized in Tables I and II, respectively.

Angular distributions were measured to distinguish between transitions of different multipolarity. Channel-selected spectra were formed by summing all detectors with $111° > \theta > 69°$ (48 detectors arranged symmetrically about $\theta = 90.0°$) or all detectors with $\theta > 142°$ (15 detectors with an average angle of $\theta = 150.3°$) where θ is the angle of the detector with respect to the beam axis. The ratio $R_\gamma = I_\gamma(90°)/I_\gamma(150°)$ was measured and normalized to the efficiency of detectors in each set. By measuring this same ratio for neighboring channels we obtained average values of $R_\gamma = 0.94(5)$ for known quadrupole transitions and $R_\gamma = 1.27(5)$ for known dipole transitions. (The transitions used for this calibration of R_γ were from ^{100}Pd [12] and ^{101}Ag [13].) The R_γ ratios of the new transitions are summarized in Table II. From this information and the coincidence relationships of the transitions we deduced a consistent set of (tentative) spin assignments as indicated in Fig. 3. Figure 4 shows a plot of R_γ for the transitions and we have indicated by open (solid) circles the transitions that have been assigned quadrupole (dipole) character. It is clear from Table II and

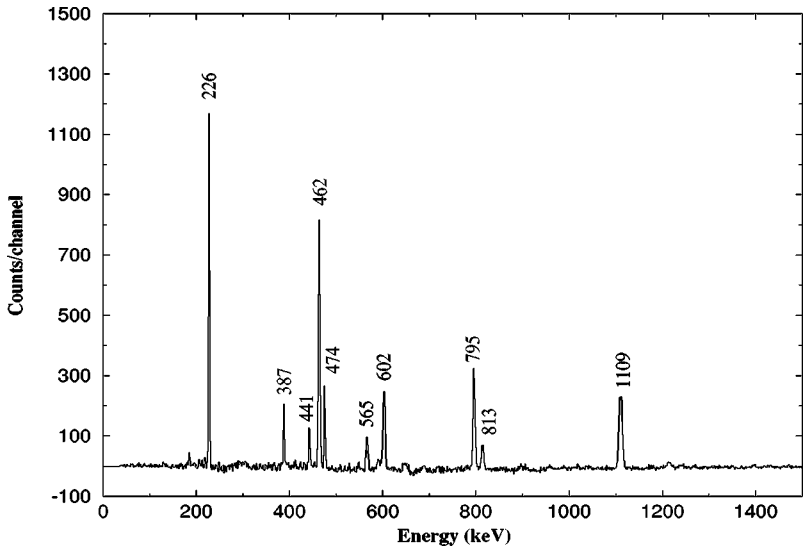

FIG. 2. Prompt spectrum formed from a single coincidence gate on the 2609 keV transition. The gate was placed on a matrix formed by requiring events to be in coincidence with one of the 296, 453, 795, 1004 keV delayed transitions in ^{100}Cd.

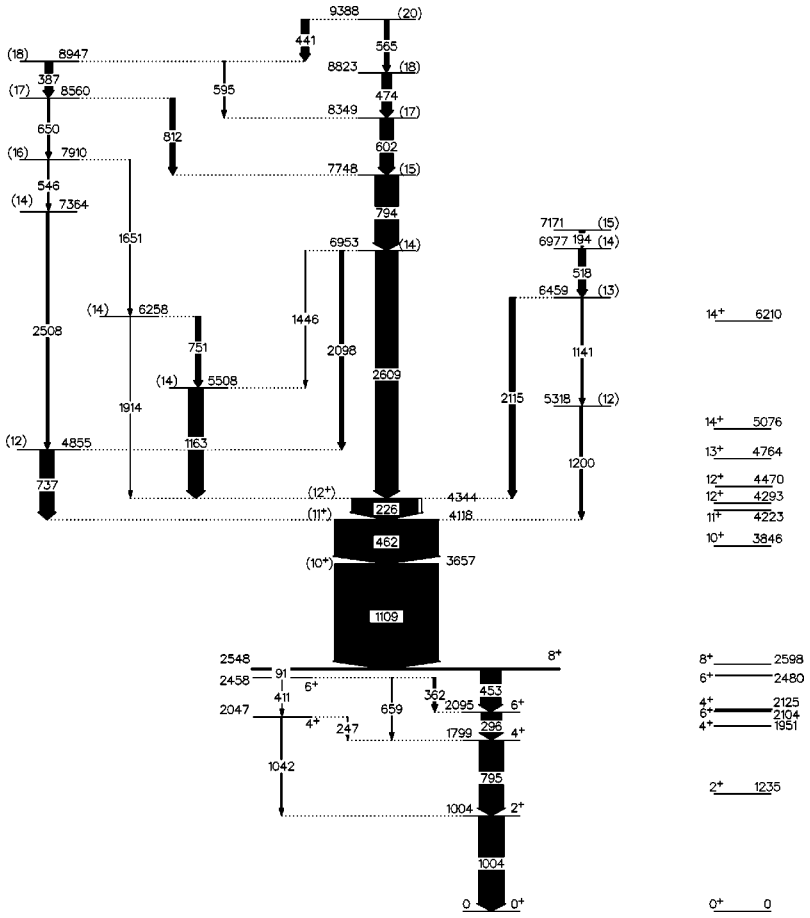

FIG. 3. Level scheme deduced from the present work. Note that all transitions above and below the 8^+ isomeric state ($t_{1/2} \simeq 60$ ns) are shown. (This level is marked by a thick bold line.) The relative intensities of transitions beneath or above this level are treated separately and have not been normalized to each other. The spins and parities are tentative. Shown to the right of the figure are the level energies from the shell-model calculation described in the text. Above $I \approx 12$ the agreement between experiment and theory becomes poor and calculated levels are not shown.

TABLE I. The transition energies E_γ (in keV) and gamma-ray intensities I_γ (measured from a delayed spectrum generated by a single coincidence gate on the 1109 keV transition, corrected for efficiency, and normalized to the 1004 keV transition) for transitions beneath the 8^+ isomer.

E_γ	I_γ
90.7(1)	5.6(8)
247.3(1)	1.0(3)
296.1(1)	88.3(26)
362.4(1)	8.6(9)
411.5(1)	3.1(4)
452.5(1)	85.1(27)
658.5(2)	4.2(5)
795.0(2)	94.3(32)
1004.1(2)	100.0(35)
1042.2(2)	2.6(6)

TABLE II. The transition energies E_γ (in keV), gamma-ray intensities I_γ (measured from a spectrum generated by a single coincidence gate on the 1109 keV gamma ray, corrected for efficiency, and normalized to the 462 keV transition), and angular distribution ratios R_γ $[=I_\gamma(90°)/I_\gamma(150°)]$ for transitions above the 8^+ isomer.

E_γ	I_γ	R_γ
193.8(1)	3.9(2)	1.21(10)
225.8(1)	37.2(5)	1.29(2)
386.9(1)	5.3(2)	1.32(7)
440.8(2)	5.4(2)	0.91(5)
461.7(1)	100.0(10)	1.30(2)
474.0(1)	6.8(3)	1.26(6)
517.8(1)	5.1(2)	1.52(8)
545.8(2)	3.7(2)	1.07(8)
564.9(2)	4.1(2)	0.89(6)
596.9(6)	1.8(5)	1.16(18)
601.6(2)	9.1(4)	1.02(5)
649.5(2)	4.9(3)	1.31(17)
736.8(2)	10.8(3)	1.30(6)
750.7(3)	5.5(3)	1.03(21)
794.5(2)	17.6(4)	1.45(3)
812.6(3)	7.2(3)	0.93(7)
1108.6(2)	—	0.85(2)
1141.1(9)	1.3(2)	1.28(14)
1163.7(3)	11.5(4)	1.03(5)
1200.7(10)	2.3(3)	—
1445.8(10)	1.5(3)	—
1652.2(11)	2.5(3)	—
1914.4(12)	1.2(2)	—
2098.7(7)	4.9(6)	1.02(12)
2116.3(12)	3.9(6)	1.36(29)
2508.4(9)	2.9(3)	1.06(15)
2609.1(4)	17.1(4)	0.75(3)

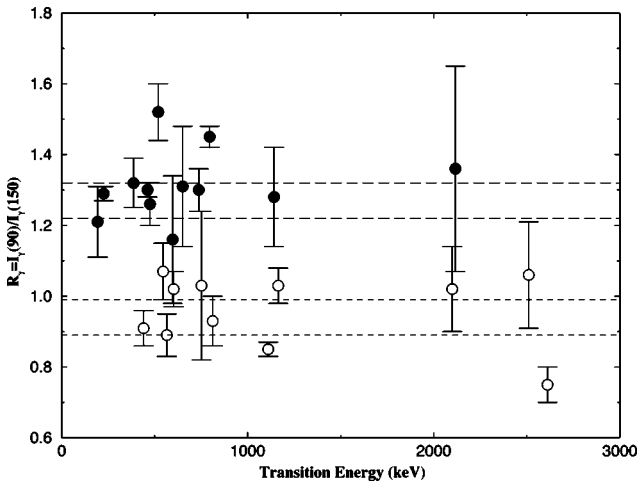

FIG. 4. The measured angular distribution ratios R_γ. Open (solid) circles indicate the transitions that have been assigned quadrupole (dipole) character. The limits indicated by the long (short) dashed lines indicate the errors in the ratios extracted for known dipole (quadrupole) transitions in neighboring nuclei (see text).

Fig. 4 that for most of the new transitions in ^{100}Cd the assigned multipolarity from the R_γ ratio is reasonable. However, for a few cases, most notably the 2609 keV transition, the R_γ values deviate from expectation. For the stronger transitions it was possible to use spectra formed for detectors located at individual values of θ for an angular correlation measurement. The extracted a_2 and a_4 coefficients were consistent with the assigned character of each of the transitions. In particular, the deduced values of $a_2=0.24(3)$ and $a_4=-0.05(3)$ for the 2609 keV transition rule out the possibility that this gamma ray has $E3$ character (which would give an expected value of $a_2\simeq 0.55$). An $E3$ polarization of the core has been seen in ^{104}Sn [14] where it results from the close proximity of the $d_{5/2}$ and $h_{11/2}$ orbitals to the Fermi surface. The measurements of angular distributions and correlations as described above make it very unlikely that any of the high-energy transitions observed in ^{100}Cd have $E3$ character.

Shell-model calculations will now be compared with the data. New calculations based on the prescription outlined in [8] are presented. The shell-model space involved protons in the $2p_{1/2}$ and $1g_{9/2}$ orbits and neutrons in the $2d_{5/2}$, $3s_{1/2}$, $2d_{3/2}$, $1g_{7/2}$, and $1h_{11/2}$ orbits. Details of the choice of one-particle energies and two-particle terms can be found in [8]. Up to approximately $12\hbar$, calculated states can be readily associated with their counterparts from the experimentally observed levels. In Table III we present the calculated excitation energies of the states and Fig. 3 also shows the calculated level energies for a direct comparison with experiment. The agreement between experiment and theory is rather good. For example, Fig. 5 shows a plot of the calculated and experimental yrast lines up to $I=14$. Also shown in Fig. 5 is the calculated yrast line from a previous shell-model study [9] involving a more restricted model space (omitting the neutron $1h_{11/2}$ orbit). (Slightly different choices of one-particle energies and two-body matrix elements were also

TABLE III. Calculated excitation energies for states in ^{100}Cd. Also included are calculated branching ratios for transitions from these states. States and transitions are given only if a corresponding experimental state or transition can be assigned. J_i^π gives the spin and parity of the state, E_i is the excitation energy of the state in MeV, J_f^π is the spin and parity of the final state to which a transition deexcites, E_f is the excitation energy of this final state in MeV, and B is the branching ratio of the observed transition and is given as a percentage of the total intensity from the initial state. No states above 12^+ are shown (see text).

J_i^π	E_i (MeV)	J_f^π	E_f (MeV)	B (%)
2_1^+	1.235	0_1^+	0.000	100.0
4_1^+	1.951	2_1^+	1.235	99.6
4_2^+	2.125	2_1^+	1.235	94.2
		4_1^+	1.951	5.7
6_1^+	2.104	4_1^+	1.951	100.0
6_2^+	2.480	4_1^+	1.951	2.3
		6_1^+	2.104	87.0
		4_2^+	2.125	10.7
8_1^+	2.598	6_1^+	2.104	1.2
		6_2^+	2.480	98.8
10_1^+	3.846	8_1^+	2.598	97.6
11_1^+	4.223	10_1^+	3.846	96.7
12_1^+	4.293	10_1^+	3.846	34.5
		11_1^+	4.223	64.5
12_2^+	4.470	11_1^+	4.223	98.5

used since this calculation was aimed specifically toward a study of all the $N=52$ isotones from ^{92}Zr to ^{100}Cd and the Hamiltonian was initially tuned to a range of nuclides on the periphery of these specific cases.) For this calculation the agreement between experiment and theory is still reasonably good but gets worse above $I=8$, perhaps reflecting an increasing influence of the $h_{11/2}$ neutron orbital.

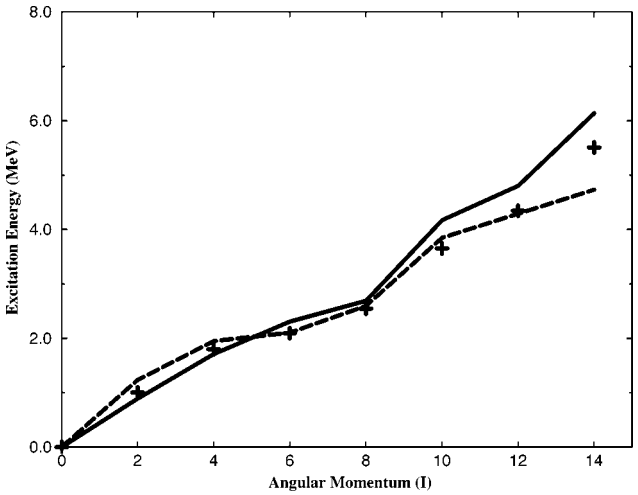

FIG. 5. Comparison of experimental and theoretical yrast level energies up to $I=14$. The crosses (+) are the experimental data. The dashed line is the calculated yrast line from the shell-model calculations based on the prescription described in [8], while the solid line is the result of the shell-model calculations of Halse [9].

TABLE IV. Experimental excitation energies of states and branching ratios for transitions in ^{100}Cd. J_i^π gives the spin and parity of the state, E_i is the excitation energy of the state in MeV, J_f^π is the spin and parity of the final state to which a transition deexcites, E_f is the excitation energy of this final state in MeV, and B is the branching ratio of the observed transition and is given as a percentage of the total transition intensity from the initial state.

J_i^π	E_i (MeV)	J_f^π	E_f (MeV)	B (%)
2_1^+	1.004	0_1^+	0.000	100(4)
4_1^+	1.799	2_1^+	1.004	100(3)
4_2^+	2.047	2_1^+	1.004	72(21)
		4_1^+	1.799	28(10)
6_1^+	2.095	4_1^+	1.799	100(3)
6_2^+	2.458	4_1^+	1.799	26(4)
		6_1^+	2.095	54(7)
		4_2^+	2.047	20(3)
8_1^+	2.548	6_1^+	2.095	85(3)
		6_2^+	2.458	15(3)
10_1^+	3.657	8_1^+	2.548	100(1)
11_1^+	4.118	10_1^+	3.657	100(1)
12_1^+	4.344	11_1^+	4.118	100(1)
12_2^+	4.855	11_1^+	4.118	100(3)

The electromagnetic matrix elements were obtained with harmonic oscillator radial wave functions with $\hbar\omega=8.58$ MeV. Effective charges of $e_\pi=1.5e$ and $e_\nu=1.5e$ were used, along with an effective $M1$ operator similar to the one used for the ^{132}Sn region in Ref. [15]. The calculated branching ratios, which do not contain corrections for the internal conversion coefficients, from a given state to lower-lying levels are also presented in Table III. These may be compared to the experimental branching ratios which are presented in a similar manner in Table IV.

The $8_1^+\rightarrow 6_1^+$ and $8_1^+\rightarrow 6_2^+$ transitions are particularly interesting. A comparison of the experimental and theoretical $B(E2)$ values is given in Table V. In the calculation, the 8_1^+ state has a rather pure $\pi g_{9/2}^{-2}$ configuration and the two 6^+ states are mixtures of mainly the $\pi g_{9/2}^{-2}$ and $\nu(d_{5/2}g_{7/2})$ configurations. The weak transition strength to the 6_1^+ state indicates that there is little mixing between the two-proton hole and two-neutron particle configurations. Indeed, there is less mixing indicated by the calculation than inferred from the experimental data. The stronger $(8^+\rightarrow 6_2^+)$ transition is dominated by the $\pi g_{9/2}^{-2}$ configuration but has some smaller neutron component. In terms of the effective charge the $E2$ matrix element is $M=16.7e_\pi+6.9e_\nu$, and with the effective charges given above the transition strength is $B(E2)$

TABLE V. Comparison of experimental and theoretical $B(E2)$ values (in e^2 fm^4) of transitions deexciting the 8^+ state (see text).

	$8^+\rightarrow 6_2^+$	$8^+\rightarrow 6_1^+$
$B(E2)$ Expt.	87(13)	0.41(3)
$B(E2)$ Theory	75	0.003

$=M^2/(2J_i+1)=75\ e^2\,\mathrm{fm}^4$ which is in reasonable agreement with the experimental value of 87(13) $e^2\,\mathrm{fm}^4$.

The proton part of this strong transition is analogous to the $8^+\rightarrow 6^+$ transition observed in ^{98}Cd [4] but the $B(E2)$ value of 11.8(3.9) $e^2\,\mathrm{fm}^4$ inferred from that experiment is much smaller than its analog in ^{100}Cd. A recent experiment [16] reports a significantly shorter lifetime for the 8^+ isomer in ^{98}Cd ($t_{1/2}=0.19(2)\ \mu$s [16] rather than 0.48(10) μs [4]) and using this value we infer a $B(E2)$ value of 29.8(31) $e^2\,\mathrm{fm}^4$. For this pure proton transition the $E2$ matrix element is $M=17.2e_\pi$ which gives $B(E2)=39\ e^2\,\mathrm{fm}^4$, in reasonable agreement with the new and larger experimental value. It will be important to confirm the lifetime in ^{98}Cd.

The new calculations presented here extend above angular momentum $I=12$ but we find that the agreement worsens and it becomes difficult to associate calculated levels with their observed counterparts. $I=14$ is the maximum spin that can be generated from two-proton holes in the $g_{9/2}$ orbital together with two neutrons in the $(g_{7/2},d_{5/2})$ orbitals relative to the $Z=N=50$ ^{100}Sn core. Other states with approximately this or higher angular momentum must be formed from configurations which involve either the $h_{11/2}$ neutron orbital or the breaking of the core. The position of the $h_{11/2}$ orbital is not well determined experimentally but is believed to lie $\simeq 2$ MeV higher than the $(g_{7/2},d_{5/2})$ orbitals (which lie close in energy to each other). Either scenario of core excitations or excitations involving the $h_{11/2}$ orbital results in a jump in the excitation energy of the resulting states. This effect is reflected in the level scheme of Fig. 3 by the number of high-energy transitions at about this excitation energy and angular momentum.

To summarize, the gamma decay of excited states in ^{100}Cd has been studied using the Gammasphere array. Very sensitive channel selection was achieved by the combination of the 4π CsI array, Microball, a set of liquid scintillator neutron detectors, and a tag on delayed gamma rays deexciting the 60 ns isomeric 8^+ state. The level scheme has been extended up to approximately $20\hbar$ in angular momentum and 10 MeV in excitation energy. The spectrum of the yrast states up to $I=14$ is generally well reproduced in shell-model calculations. Around the excitation energy and angular momentum of this state, high-energy ($E_\gamma\simeq 2.0-2.6$ MeV) transitions are observed. These transitions can be viewed as a ''fingerprint'' of either core excitations or excitations involving $h_{11/2}$ neutrons. It is clear that a full quantitative description of the decay scheme requires extended shell-model calculations. Indeed, the recent advances in gamma-ray spectroscopy of nuclei near ^{100}Sn are clearly outstripping the theoretical descriptions and it is our hope that experimental efforts such as presented here will encourage renewed theoretical effort.

We would like to express our gratitude to the crew and staff of ATLAS and Andrzej Lipski (SUNY) for making the high-quality target foils. The help of John Greene (ANL) with the targets for the run was invaluable. Many thanks to the University of Manchester (U.K.) and University of Pennsylvania groups who provided and set up the neutron detectors prior to our experiment. This work has been supported in part by the U.S. DOE under Contracts No. DE-AC03-76SF00098 (LBNL), W-31-109-ENG-38 (ANL), and DE-FG02-88ER-40406 (WU). The SUNY at Stony Brook group acknowledges partial support from the U.S. NSF. B.A.B. would like to acknowledge support from the U.S. NSF under Grant No. PHY-9605207. Two of us (R.M.C. and R.W.) would like to acknowledge partial support from NATO under Grant No. CRG 972142.

[1] R. Schneider *et al.*, Z. Phys. A **348**, 241 (1994).
[2] M. Lewitowicz *et al.*, Phys. Lett. B **332**, 20 (1994).
[3] M. Chartier *et al.*, Phys. Rev. Lett. **77**, 2400 (1996).
[4] M. Górska *et al.*, Phys. Rev. Lett. **79**, 2415 (1997).
[5] M. Lipoglavsek *et al.*, Z. Phys. A **356**, 239 (1996).
[6] M. Lipoglavsek *et al.*, Phys. Lett. B **440**, 246 (1998).
[7] M. Górska *et al.*, Z. Phys. A **350**, 181 (1994).
[8] B. Alex Brown and K. Rykaczewski, Phys. Rev. C **50**, R2270 (1994).
[9] P. Halse, J. Phys. G **19**, 1859 (1993).
[10] I.Y. Lee, Nucl. Phys. **A520**, 641c (1990).
[11] D.G. Sarantites, P.-F. Hua, M. Devlin, L.G. Sobotka, J. Elson, J.T. Hood, D.R. LaFosse, J.E. Sarantites, and M. R. Maier, Nucl. Instrum. Methods Phys. Res. A **381**, 418 (1996).
[12] S.K. Tandel, S.B. Patel, Pragya Das, R.P. Singh, and R.K. Bhowmik, Z. Phys. A **357**, 3 (1997).
[13] B. Crowell *et al.*, Phys. Rev. C **45**, 1564 (1992).
[14] M. Görska *et al.*, Phys. Rev. C **58**, 108 (1998).
[15] G.N. White *et al.*, Nucl. Phys. **A644**, 277 (1998).
[16] R. Grzywacz, *ENAM98: Exotic Nuclei and Atomic Masses*, edited by B.M. Sherrill, D.J. Morrissey, and Cary N. Davids (AIP, Woodbury, NY, 1998), p. 430 .